

Water temperature sensitivity under climatic change: comparison between mountain and lowland rivers in the Loire basin

A. BEAUFORT¹, V. BUSTILLO², F. CURIE¹, F. MOATAR¹, A. DUCHARNE³ & D. THIERY⁴

*1 Laboratoire GéoHydrosystèmes Continentaux (GeHCO) – Université François Rabelais, Faculté des Sciences et Techniques, Parc de Grandmont, 37200 Tours, France
aurelien.beaufort@univ-tours.fr*

2 CESBIO UMR 5126 (CNES-CNRS-IRD-UPS), IUT Paul Sabatier, Antenne d'Auch-24, rue d'Embaquès 32000 Auch, France

3 Sisyphé (UMR 7619), Université Pierre et Marie Curie, 4 place Jussieu, 75252 Paris Cedex 05, France

4 Bureau de Recherches Géologiques et Minières (BRGM), 3 avenue Claude-Guillemain-BP 36009 45060 Orléans Cedex 2, France

Abstract In a context of climate change, the capacity to forecast the thermal regime of rivers is a major challenge for water resource management and for aquatic ecosystem preservation. To address the geographic distribution of daily water temperature within the entire drainage network of the Loire basin (110 000 km²), we based our work on the equilibrium temperature concept, as developed in the ICC-Hydroqual project. Sixty-eight sub-basins (300 to 3000 km²) are delineated, in which Strahler orders are considered to behave similarly. The model uses a heat balance with five terms based on meteorological variables provided by Safran interpolation analysis (8 km × 8 km) of Météo-France. The simulation of the river discharge was performed by means of the semi-distributed hydrological model EROS. The performance of the model for simulating water temperature over the last 33 years (1974–2007) for 71 sampling stations led to median RMSE = 1.97°C. Thermal regime at the end of the 21st century (2080–2100) was simulated using 13 changing climate (A1B) and hydrological scenarios derived by the EROS model. The combination of these scenarios results in the same increase of the mean annual temperature by 2.2°C (±0.6°C). The increase of the mean monthly temperature is similar for mountain rivers (mean basin elevation 600 m) and for lowland rivers (mean basin elevation 130 m). The water temperature increases by 3.0°C (±0.9°C) in spring and autumn and by 2.6°C (±0.7°C) in summer. This limited increase in summer can be explained by the rise of the energy loss by the net long-wave radiation and by the evaporative heat flux, correlated with a reduction of the increase of the net short-wave radiation.

Key words thermal models; climate changes; equilibrium temperature; mountain and lowland rivers; Loire Basin; France

INTRODUCTION

Climate change is likely to have a major impact on the physico-chemical and ecological quality of hydrosystems through a rise in water temperature and modification of flow (Arnell, 1999; Ducharne *et al.*, 2008). More specifically, the temperature of rivers determines oxygen solubility, the kinetics of biological and chemical reactions, the distribution of fish, and hence influences the functioning of aquatic ecosystems. The heat balance of rivers is influenced by many factors, including atmospheric conditions, topography, riverine vegetation, river flow and heat flux arising from river beds (Caissie, 2006; Webb *et al.*, 2008). Physically-based models are preferred to statistical models to estimate the impact of climate change on the heat balance of rivers, in spite of the large quantity of data required (hydrological, geomorphological and meteorological), because they make it possible to extrapolate changes based on their underlying conditions (St-Hilaire *et al.*, 2003; Caissie *et al.*, 2007; Bustillo *et al.*, 2012). In this article, we use a model based on the concept of equilibrium temperature proposed by Edinger (1968), which is simpler to implement at a regional scale and which gives similar results to those obtained with a more traditional approach (Bustillo *et al.*, 2012). The equilibrium is recognized as an appealing way to simulate river temperatures (Caissie *et al.*, 2005). The main aim of this work is to study the impact of climate change on the heat balance of rivers on a regional scale. The Loire basin (110 000 km²) was selected on account of its contrasting features in terms of morphology (slopes of 0.3 to 67 m/km), lithology (sedimentary and crystalline domain) and climate (annual precipitation of 600 to 1300 mm). Flow and temperature of the basin rivers were simulated for the present time (1970–2007)

(hereafter called PT), at mid-century (2046–2065) (hereafter called MC) and at the end of the century (2081–2100) (hereafter called EC) based on 13 A1B climate projections of the 4th GIEC report. In this article, we compare the hydrological and heat responses of two catchments in similar lithological settings but with different meteorological and geomorphological features: (1) the Doulon basin (250 km²) in the Massif Central, and (2i) the Oudon basin (150 km²) on the Armorican plain. Hydrological and meteorological features were analysed with the aim of estimating their influences on the regulation of the water temperature under climate change.

MODELS AND DATA

The approach developed here is based on combining a semi-distributed EROS hydrological model (Thiéry & Montzopoulos, 1995) and a thermal model developed as part of the ICC-Hydroqual project (2010). The Loire basin has been divided into 68 sub-basins of between 300 and 3000 km² (Fig. 1). Daily flows are simulated at the outlet of these 68 sub-basins according to meteorological forcing derived from the SAFRAN database (8 km × 8 km) (Quintana-Segui *et al.*, 2008). The SAFRAN database provided daily data covering France at 8-km resolution for the period 1970–2007 for the following near-surface parameters: air temperature (T_a , 2 m above the soil surface, °C), specific humidity (Q , 2 m above the soil surface, kg/kg), snowfall (S , mm/s), rainfall (R , mm/s), wind velocity (W , 10 m above the soil surface, m/s), global radiation (R_g , W/m²), and atmospheric radiation (R_a , W/m²). For simulations of the future, the same meteorological variables were obtained from 13 A1B climate projections of the 4th GIEC report. The thermal model is based on the resolution of an energy balance which includes exchanges with the atmosphere and water tables, and the upstream–downstream propagation of the heat signal based on average morphological features (Fig. 2). It simulates daily temperature within the 68 sub-basins for each Strahler stream order.

Water temperature simulation was carried out in two stages: (1) determining the hydraulic conditions, and (2) calculating the 0D temperature which only taking account of inertial factors (river depth) but without including the upstream-downstream propagation of thermal signal.

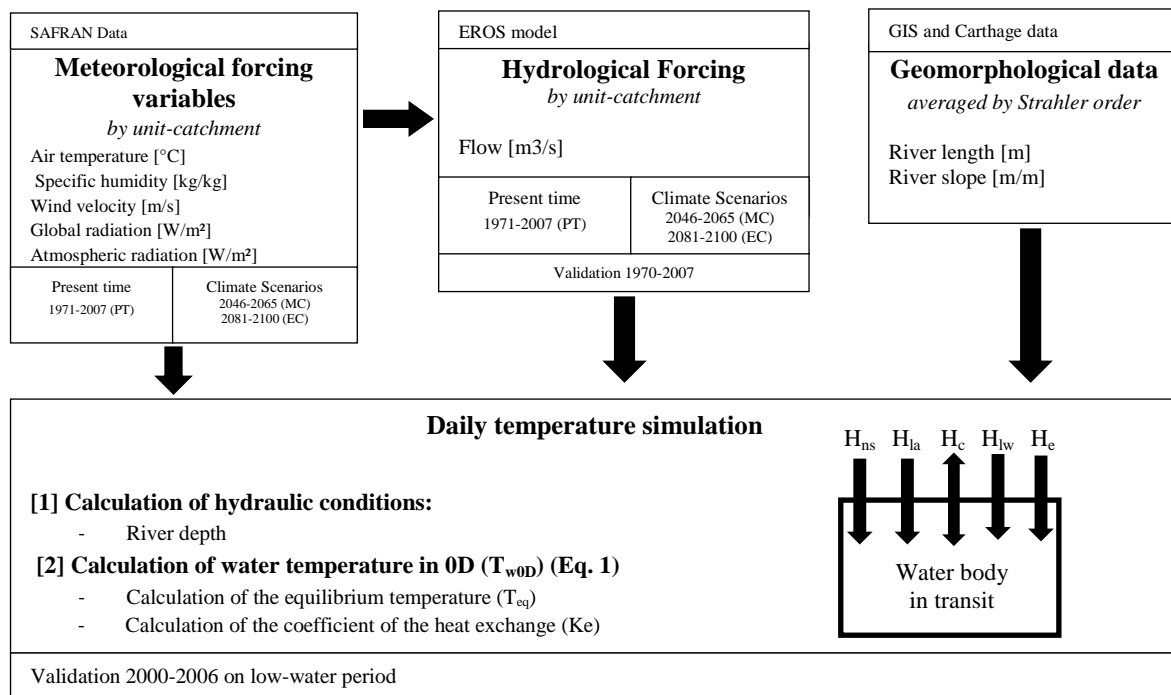


Fig. 1 Principle of the model used to simulate water temperature.

Calculating the hydraulic characteristics of reach categories

This stage involved determining the depth of 544 categories of reach (68 sub-basins \times 8 Strahler orders) and the average flow in these reaches. The width and the depth were determined using the ESTIMKART application which takes account of the median flow and the daily flow of the reaches (Lamouroux *et al.*, 2010). The main characteristics (length and slope) of the drainage network were extracted from the CARTHAGE (CARtographie THématique des AGences de l'Eau et du ministère de l'environnement) database and the BD ALTI[®] 25-metre resolution DTM dataset.

Calculating 0D temperature at the outlets of the 68 sub-basins and for each Strahler order

First, we determined the equilibrium temperature (T_e) defined when the algebraic sum of the five energy flows is zero. These are the net short-wave radiation (H_{ns}), incident long-wave radiation (H_{la}), outgoing long-wave radiation (H_{lw}), the convective heat flux (H_c), and the energy used for evaporation/condensation (H_e) (Table 1). Next, the Edinger equation (equation (1)) was computed at a daily time step to define the 0D temperature (T_{w0D}):

$$T_{w0D}(t) = T_e(t) + [T_w(t - \Delta t) - T_e(t)] \times \exp\left[\frac{-K_e(t)}{\rho_w C_p D(t)} \times \Delta t\right] \quad (1)$$

where $T_w(t)$ is the temperature of the river in °C at day t , ρ_w is the water density in kg/m^3 , C_p is the specific heat of the water = 4180 J/kg/K, $D(t)$ is the average depth (m), and K_e is the coefficient of heat exchange at time t , derived from Edinger's formulation:

$$k_e(t) = 4\varepsilon\sigma(T_{w0D}(t) + 237.15)^3 + f(w) \times \left(0.62 + 6.11 \times \frac{17.27 \times 237.3}{(237.3 + T_{w0D}(t))^2}\right) \times \exp\left[\frac{17.27 \times T_{w0D}(t)}{237.3 + T_{w0D}(t)}\right] \quad (2)$$

where K_e is expressed in $\text{W/m}^2/\text{K}$ at day t , $f(w)$ is an empirical function expressed in $\text{W/m}^2/\text{mb}$ (Thomann & Mueller, 1987) according to wind speed and is expressed as $f(w) = 9.2 + 0.46W_T^2$ where W is the wind speed in m/s measured 7 m above the ground. A shading factor (SF), corresponding to a coefficient of reduction of the overall incident radiation (H_{ns}) is determined by calibration.

Table 1 Parameters used to determine the energy flows occurring at the water/air interface

Heat terms (W/m^2)	Formulation	Parameters	Assumptions
Net short-wave radiation (H_{ns})	$H_{ns} = (1 - Alb) \times Rg \times (1 - SF)$	Alb = Surface water albedo Rg = Global radiation (W/m^2) SF = Shadow factor	$Alb = 0.06$ SF (Calibrate) : $M=0.25$; $P=0.05$
Long-wave radiation (H_{la})	$H_{la} = 0.97 \varepsilon_a \sigma (T_a + 273.15)^4 \times (1 + 0.22 \text{Cld}^{2.75})$	ε_a : Clear-sky atmospheric emissivity σ : Boltzmann constant T_a : Air temperature (°C) Cld : Cloud cover fraction	$\varepsilon_a = \text{constant}$ $\sigma = 567 \times 10^{-8} \text{ W/m}^2/\text{K}^4$
Long-wave emitted radiation (H_{lw})	$H_{lw} = \varepsilon_a \sigma (T_w + 273.15)^4$	T_w : Water temperature (°C)	$\varepsilon_a = \text{constant}$ $\sigma = 5.67 \times 10^{-8} \text{ W/m}^2/\text{K}^4$
Convection (H_c)	$H_c = B f(w) (T_a - T_w)^4$	B : Bowen's coefficient $f(w) = aw + b$: wind function w : wind speed at 7 m	$a = 0.46$ and $b = 9.2$ $B = 0.62 \text{ mb}^\circ\text{K}^{-1}$
Evaporation (H_e)	$H_e = f(w) (e_s - e_a)$	e_a : water vapour pressure in air (mb) e_s : saturation vapour pressure for T_w (mb)	Magnus-Tetens approximation: $e_s = 6.11 \times \exp\left[\frac{17.27 T_w}{237.3 + T_w}\right]$

STUDY SITE AND DATA

We selected two basins for which hourly temperature data during the summer period are available: (1) the Doulon basin (250 km², hereafter called M for “mountain”), located in the Massif Central, has a high relief (altitude 10–1849 m), and (2) the Oudon basin (150 km², hereafter called P for “plain”), located on the plain on the Massif Armorican. The two basins form part of sub-basins no. 9 (Allier to Vic-le-Comte, called M*) and no. 65 (Oudon to Andigné, called P*). The lithology of basin P is composed of 80% sandstone and schist forming the bedrock of the Massif Armoricain. Basin M is composed of the granite forming the bedrock of the Massif Central. Specific interannual flows (QA), low-water flows (Q90), and the flow profiles of the two rivers are similar (approx. 7 and 20 L/s/km² for QA and Q90), indicating similar hydrological behaviour.

The interannual air temperatures (1971–2007), annual and summer, are 2.8°C and 1.9°C higher in basin P than in basin M.

The outlets of basins M and P are equipped with hourly temperature sensors for the summer period (June to September 2000 to 2006). The mean summer water temperature of basin P is 0.8°C higher than that of basin M. The diurnal temperature range is greater in basin M (3.7°C) than in basin P (1.8°C).

Table 2 Characteristics of sub-basins P and M.

BV	Area (km ²)	Averaged altitude (m)	Averaged slope (m/km)	T _{air} Summer (°C)	T _{air} Annual (°C)	T _{eau} summer (°C)	T _{eau} Diurnal amplitude (°C)	Specific flow (L/s/km ²)
M	250	500	18	16.3	8.5	16.4	3.7	7.3
P	150	50	3	18.2	11.3	17.6	1.8	6.7

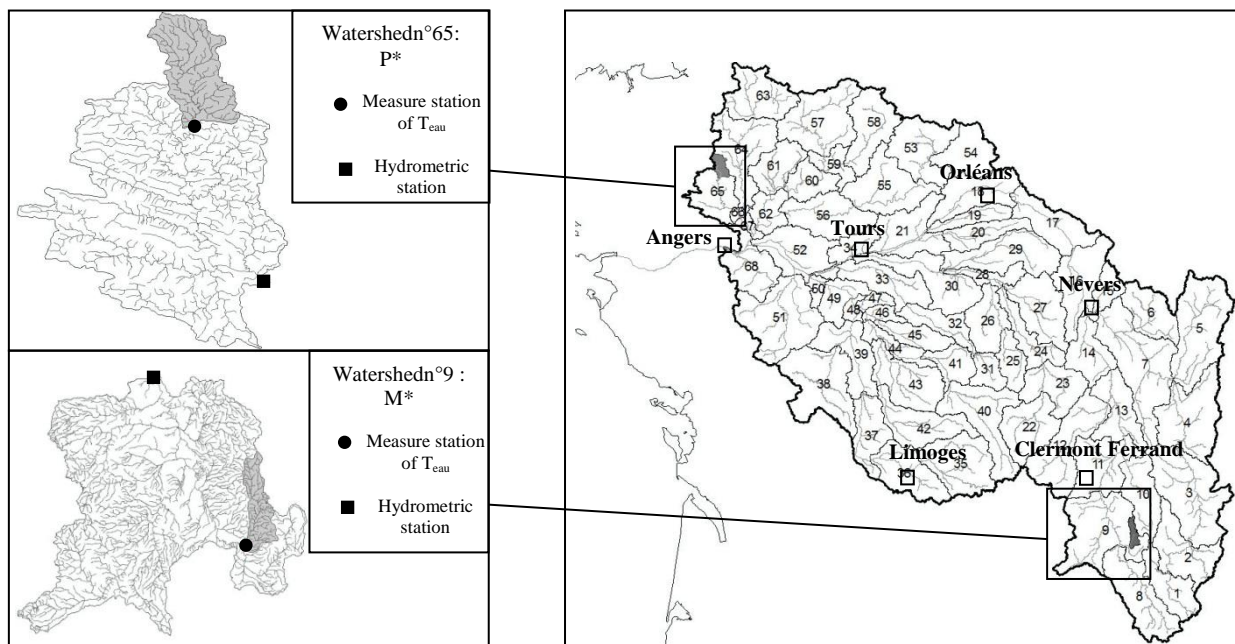


Fig. 2 Map location of the P and M basins (Grey) in the Loire River basin.

RESULTS AND DISCUSSION

Performance of the hydrological and thermal models

To test the performance of the hydrological model at high, medium and low flows, Nash criteria were calculated on discharge values (C1), on the square root of the discharge (C2), and the logarithms of the discharges (C3). The performances of the hydrological model at the outlet of the

47 hydrometric stations used for the calibration are good (the medians of the criteria range between 0.84 and 0.87). Moreover, for the Nash criterion C3, 75% of the sub-basins were between 0.77 and 0.93 during the low-water period, which is of particular interest for this study. Likewise, for basins M* and P*, flows are very well simulated, because the criteria come within the upper quartile of performances (C1 = 0.80; C2 = 0.90; C3 = 0.70 for the least-well simulated basin).

The performance of the thermal model was analysed for 67 hourly monitoring stations of ONEMA, with Strahler orders of between 1 and 8 (data for June to September, 2000–2006). At all these stations, the median bias ($T_{\text{modeled}} - T_{\text{measured}}$) is zero, the standard deviation of errors is 1.6°C. For study basins M and P (Fig. 3), biases are -0.4 and -0.2°C, respectively, with standard deviations of 1.8 and 1.1°C over the validation period (2000–2004).

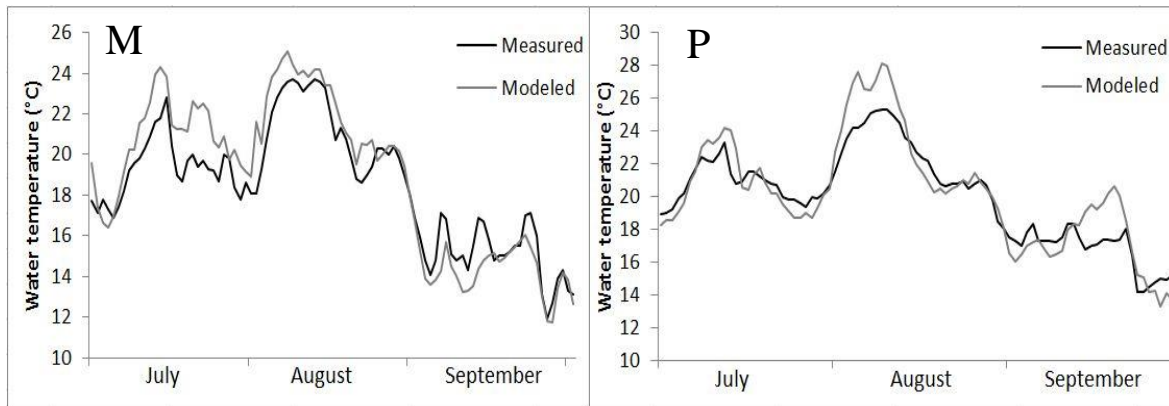


Fig. 3 Results of measured and modeled daily water temperature in M and P for the period 1 July 2003 to 30 September 2003.

The hydrological model faithfully represents flows in basin P for a dry year (2003) and a wet year (2000), with biases of -0.1 L/s/km² and 0.3 L/s/km² respectively, and standard deviations of 1.2 L/s/km² and 0.8 L/s/km². The performances of the thermal model for 2000 and 2003 are in the same order of magnitude as for the validation period of the model, with biases of -0.1 and 0.1°C respectively, and standard deviations of 1.7 and 1.6°C (Fig. 4).

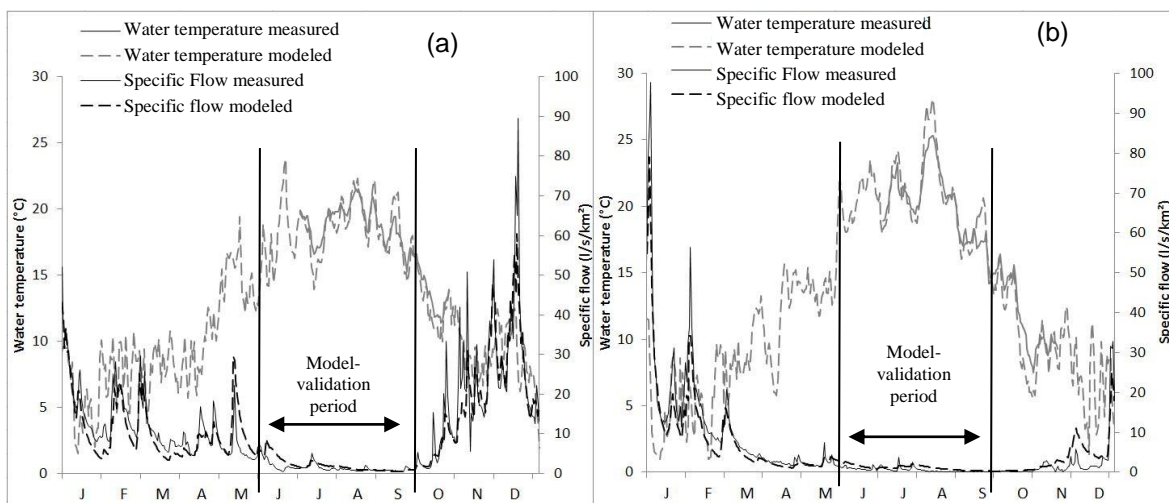


Fig. 4 Results of measured and modeled daily water temperature and of the specific flow in P for 2000 (a) and 2003 b).

Response of the heat and hydrological balance of the rivers to climate projections during the 21st century

The EROS model simulates a steady decrease in annual flows at mid-century (MC) ($-20\% \pm 10\%$) and at the end of the century (EC) ($-35\% \pm 15\%$). The uncertainty values represent the standard deviation of flow simulations based on 13 global circulation models (GCMs) including A1B climate projections. However, this decrease is greater at low-water periods. This trend can be seen in both basins M* and P* where flows decrease by -45% ($\pm 13\%$) between June and September (Fig. 5). The curve of present median flows lies above the 90% percentile of the simulations carried out for climate projections during low-water periods.

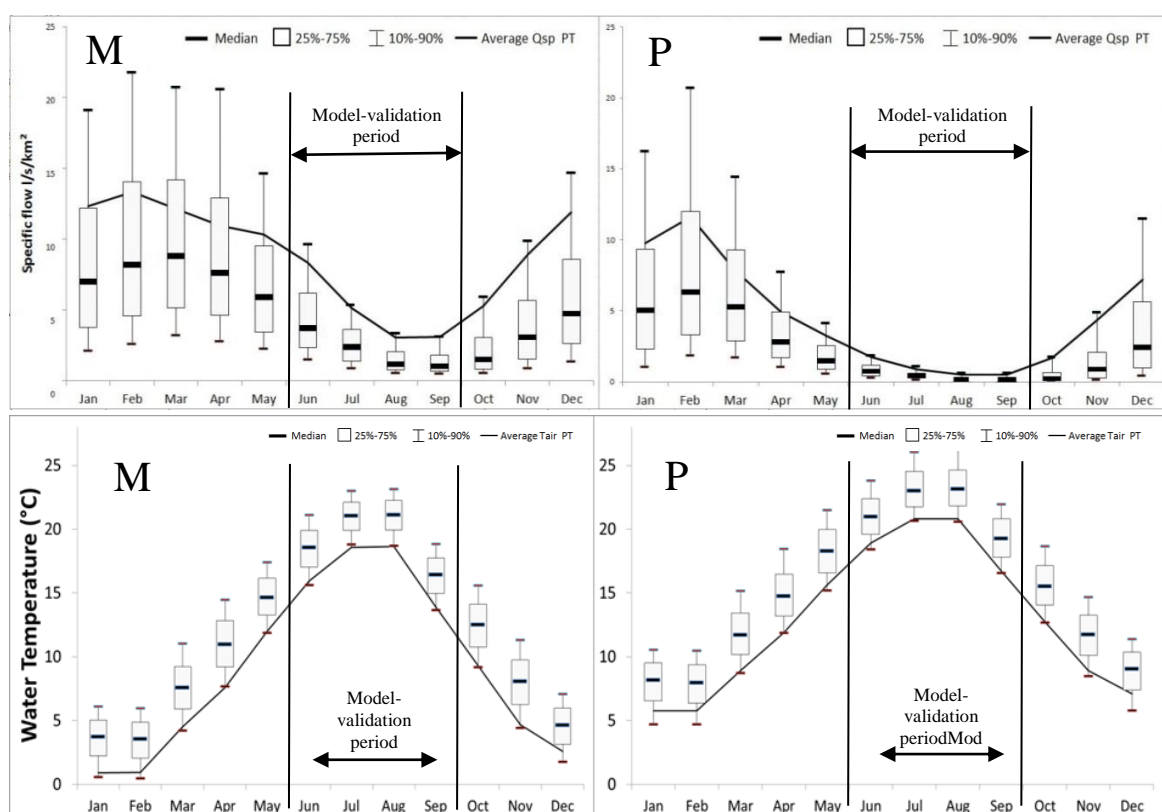


Fig. 5 Mean monthly specific flow and mean monthly water temperature simulated in M and P at the end of the 21st century (EC) (whiskers boxes) compared to the present period (solid line).

At the Loire basin scale, the thermal model simulates an increase of the water temperature by 2.2°C ($\pm 0.5^{\circ}\text{C}$) at MC and by 2.9°C ($\pm 0.7^{\circ}\text{C}$) at EC. The uncertainty values represent the standard deviation of water temperature simulations based on 13 A1B climate projections. For basins M and P, mean annual water temperature increases respectively by 2°C ($\pm 0.5^{\circ}\text{C}$) and 1.8°C ($\pm 0.8^{\circ}\text{C}$) at MC, and by 2.8°C ($\pm 0.5^{\circ}\text{C}$) and 2.5°C ($\pm 0.8^{\circ}\text{C}$) at EC (Fig. 5). This increase is robust particularly for the summer. The 10% percentiles of the simulations for scenario A1B for the end of the century are below or near the current median flow regimen. The behaviour of the water temperature anomalies (difference of monthly EC – PT means) is identical in the two basins during the year (Fig. 6). The increase of the water temperature seems more important in spring and autumn ($+3.0^{\circ}\text{C} \pm 0.9^{\circ}\text{C}$) than in summer ($+2.6^{\circ}\text{C} \pm 0.7^{\circ}\text{C}$). Several factors may explain the difference in water temperature anomalies between summer, spring and autumn: an increase of the net heat flux or a decrease of river flow involving a reduction of the river depth.

We have seen that flows decrease by -45% ($\pm 13\%$) between June and September at EC, which led to a decrease of river depth by 12% in basin M and by 5% in basin Van Vliet *et al.*, (2011) have shown that a decrease in discharge of 40% resulted in a slight increase of river water

temperature by $+0.8^{\circ}\text{C}$ and it was particularly accentuated during dry and warm spells at a global scale. In this study, the decrease of the river depth in summer (0.08 m for M and 0.05 m for P) does not have any impact on the monthly average water temperature. However, maximum and minimum depths will be reduced by 15% in the two basins, involving a decrease of the thermal inertia of rivers and an increase of the water temperature during the warm-up period.

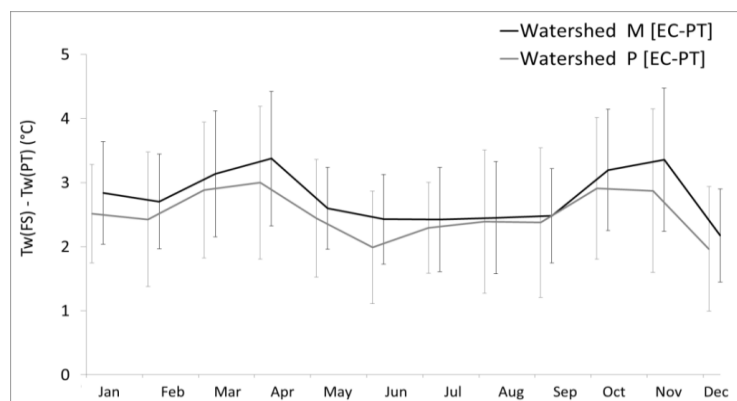


Fig. 6 Water temperature anomalies (difference of monthly EC – PT means). The error bar corresponds to the standard deviation of water temperature anomalies for 13 GCMs including A1B climate projections

The increase of the net heat flux will lead to rise of the equilibrium temperature. Bustillo *et al.* (2013) have shown an increase of equilibrium temperature of 3.2°C on the Loire River at the EC, largely due to the increase of the air temperature ($+3.6^{\circ}\text{C}$). For basins M and P, mean annual water temperature increases by 2.8°C ($\pm 0.5^{\circ}\text{C}$) and 2.5°C ($\pm 0.8^{\circ}\text{C}$), respectively, and the air temperature increases by 3°C . However the air temperature increases by 2.8°C in spring and by 3.3°C in summer and autumn. Water temperature anomalies (Fig. 6.) do not follow exactly the same trend as the air temperature and we can expect that other climatic parameters are going to limit the increase of water temperature during summer. The net short-wave radiation (H_{ns}) is the major contributor to the surface of water heat gain in the two basins. At the EC, this heat flux is going to increase by 20% in spring and autumn, while in summer this increase is limited to 5% (Table 3). The heat gain in summer will be limited leading to less increase of the equilibrium temperature. The net long-wave radiation ($H_{nlw} = H_{la} - H_{lw}$) is the main contributor to energy loss at the water surface (60% of the energy loss). At EC, the mean annual value of this heat flux rises to 8% on basin M and to 3% on basin P. The second contributor of energy loss is the evaporative heat flux (H_e) (35% of the energy loss). At EC, the mean monthly evaporation increases of 30% on basin M and by 20% on basin P and will become the main contributor to energy loss in summer (Table 3). The increased energy loss by evaporation contributes to limit the rise of the water temperature, especially in summer. The sensible heat flux (H_c) is the third contributor to energy loss and represents 5% of the energy loss at PT and 10% in summer at EC (Table 3). However, the impact of this heat flux on the water temperature is very small. Finally, we can explain the smaller increase of the water temperature in summer by the rise of energy loss due to net long-wave radiation and by the evaporative heat flux, correlated with a reduction of the increase of the net short-wave radiation. In summer, the surface water heat gain will be smaller than in spring or autumn, which leads to reduction of the net heat flux and decrease of the equilibrium temperature.

The general increase of river water temperature will modify the fish community structure and fish migration (Schindler, 2001). For example, sedentary fish, belonging to the *Cyprinidae* family, have a reproduction threshold of 16°C . Over the PT (1971–2007), the over-run of this threshold occurs at the beginning of June in basin P and in mid-June in basin M. At the EC (2081–2100), we simulate an over-run of the threshold of 32 days earlier than PT for M, and 26 days earlier than PT for P. If these projections are accurate, it should be expected that a strong change of the actual ecological balance may arise.

Table 3 Mean seasonal heat fluxes (W/m^2) in M and P at present time (PT) and at the end of the 21st century (EC).

Heat Flux [W/m^2]	Basin M								Basin P							
	H_{ns}		H_{nlw}		H_c		H_e		H_{ns}		H_{nlw}		H_c		H_e	
	PT	EC(Gain)	PT	EC(Gain)	PT	EC(Gain)	PT	EC(Gain)	PT	EC(Gain)	PT	EC(Gain)	PT	EC(Gain)	PT	EC(Gain)
Winter	35	35(-)	-37	-37(-)	6	9(+33%)	-4	-5(-20%)	38	36(-6%)	-22	-18(+18%)	-3	-3(-)	-13	-17(-24%)
Spring	93	108(+14%)	-56	-60(-7%)	-6	-8(+25%)	-27	-37(-27%)	127	147(+24%)	-51	-55(-8%)	-20	-21(-5%)	-53	-69(-24%)
Summer	126	132(+5%)	-62	-62(-)	-7	-7(-)	-52	-65(-20%)	168	173(+3%)	-58	-58(-)	-19	-11(+43%)	-91	-104(-13%)
Autumn	57	72(+21%)	-44	-48(-8%)	1	1(-)	-17	-28(-30%)	70	90(+23%)	-31	-37(-17%)	-5	-5(-)	-34	-50(-32%)

Finally, we have seen that the thermal regime of rivers located in mountain and in lowland regions have the same response under climate change with a similar increase of the water temperature at the EC. It may seem that the geomorphological parameters of rivers have limited influence on the regulation of water temperature in this thermal model. To improve the performance of the water temperature simulation it would be efficient to implement a more precisely discretized thermal model. This approach will permit the taking into account of the geomorphological and meteorological parameters for each river section with the goal of better estimating the evolution of their thermal regime under climate change.

Acknowledgements This work was realised in the course of work for a thesis funded by the Office National de l'Eau et des Milieux Aquatiques (ONEMA). It also benefitted from financial supports by the Fonds Européen de développement Régional (FEDER), the Etablissement Public Loire (EPL) and the water Agency of Loire Bretagne (AELB). Thanks are due to Météo-France for the SAFRAN database.

REFERENCES

- Arnell, N.W. (1999). The effect of climate change on hydrological regimes in Europe: a continental perspective. *Global Environmental Change* 9, 5–23.
- Bustillo, V., Moatar, F., Ducharne, A., Thiéry, D. & Poirel, A. (2012) A multimodel comparison for assessing water temperatures under changing climate conditions via the equilibrium temperature concept: case study of the Middle Loire River, France. *Hydrological Processes* doi: 10.1002/hyp.9683.
- Caissie, D. (2006) The thermal regime of rivers: a review. *Freshwater Biology* 51, 1389–1406.
- Caissie, D., Satish, M.G. & El-Jabi, N. (2005) Predicting river water temperatures using the equilibrium temperature concept with application on the Miramichi River catchments (New Brunswick, Canada). *Hydrological Processes* 19, 2137–2159.
- Caissie, D., Satish, M.G. & El-Jabi, N. (2007) Predicting water temperatures using a deterministic model: Application On Miramichi River catchments (New Brunswick, Canada). *Journal of Hydrology* 336(3), 303–315.
- Ducharne, A. (2008) Importance of stream temperature to climate change impact on water quality. *Hydrology and Earth System Science* 12, 797–810.
- Edinger, J.E., Duttweiler, D. & Geyer, J. (1968) The response of water temperatures to meteorological conditions. *Water Resources Research* 4, 1137–1143.
- Lamouroux, N., Pella, H., Vanderbecq, A., Sauquet, E. & Lejot, J. (2010) Estimkart 2.0: Une plate-forme de modèles écohydrologiques pour contribuer à la gestion des cours d'eau à l'échelle des bassins français. Version provisoire. Cemagref – Agence de l'Eau Rhône-Méditerranée-Corse – Onema210.
- Mohseni, O., Stefan, H.G. & Erickson, T.R. (1998) A non-linear regression model for weekly stream temperatures. *Water Resources Research* 10, 2685–2692.
- Quintana-Seguí, P., Le Moigne, P., Durand, Y., Martin, E., Habets, F., Baillon, M., Canellas, C., Franchisteguy, L. & Morel, S. (2008) Analysis of near surface atmospheric variables: validation of the SAFRAN analysis over France. *Journal of Applied Meteorology and Climatology* 47, 92–107.
- Schindler, D.W. (2001) The cumulative effects of climate warming and other human stresses on Canadian freshwater in the new millennium. *Canadian Journal of Fisheries and Aquatic Sciences* 58, 18–29.
- St-Hilaire, A., Morin, G., El-Jabi, N. & Caissie, D. (2000) Water temperature modeling in a small forested stream: implication of forest canopy and soil temperature. *Canadian Journal of Civil Engineering* 27, 1095–1108.
- Thiéry, D. & Moutzopoulos, C. (1995) Un modèle hydrologique spatialisé pour la simulation de très grands bassins: le modèle EROS formé de grappes de modèles globaux élémentaires. In: *VIIIèmes journées hydrologiques de l'ORSTOM "Régionalisation en hydrologie, application au développement"* (ed. by Le Barbé & E. Servat), ORSTOM Editions. 285–295.
- Thomann, R.V. & Mueller, J.A. (1987) *Principles of Surface Water Quality Modeling and Control*. Harper & Row, New York.
- Van Vliet, M.T.H., Ludwig, F., Zwolsman, J.J.G., Weedon, G.P. & Kabat, P. (2011). Global river temperatures and sensitivity to atmospheric warming and changes in river flow. *Water Resources Research*, 47, W02544, doi:10.1029/2010WR009198.
- Webb, B.W., Hannah, D.M., Dan Moore, R., Brown, L.E. & Nobilis, F. (2008) Recent advances in stream and river temperature research. *Hydrological Processes*, 22, 902–918.